Short-wavelength MEMS-tunable VCSELs

Garrett D. Cole,[1,*] Elaine Behymer,[1] Tiziana C. Bond[1,*], and Lynford L. Goddard,[1,2]

[1]*Center for Micro- and Nanotechnologies, Lawrence Livermore National Laboratory, Livermore, CA 94550, USA*
[2]*Currently with the Department of Electrical and Computer Engineering, Micro and Nanotechnology Laboratory, University of Illinois at Urbana-Champaign, Urbana, IL 61801.*
[*]*Corresponding authors: cole35@llnl.gov, bond7@llnl.gov*

Abstract: We present electrically-injected MEMS-tunable vertical-cavity surface-emitting lasers with emission wavelengths below 800 nm. Operation in this wavelength range, near the oxygen A-band from 760−780 nm, is attractive for absorption-based optical gas sensing. These fully-monolithic devices are based on an oxide-aperture AlGaAs epitaxial structure and incorporate a suspended dielectric Bragg mirror for wavelength tuning. By implementing electrostatic actuation, we demonstrate the potential for tuning rates up to 1 MHz, as well as a wide wavelength tuning range of 30 nm (767−737 nm).

OCIS codes: (250.7260) Vertical cavity surface emitting lasers; (140.3600) Lasers, tunable; (230.4685) Optical microelectromechanical devices.

References and links

1. D. C. Hovde and C. A. Parsons, "Wavelength modulation detection of water vapor with a vertical-cavity surface-emitting laser," Appl. Opt. **36**, 1135–1138, (1997).
2. I. Linnerud, P. Kaspersen, and T. Jæger, "Gas monitoring in the process industry using diode laser spectroscopy," Appl. Phys. B **67**, 297–305 (1998).
3. V. Weldon, J. O'Gorman, J. J. Pérez-Camacho, and J. Hegarty, "Oxygen sensing using single-frequency GaAs-AlGaAs DFB laser diodes and VCSELs," Electron. Lett. **32**, 219–221 (1996).
4. M. Lackner, G. Totschnig, F. Winter, R. Shau, M. Ortsiefer, J. Rosskopf, and M. C. Amann, "Demonstration of methane spectroscopy using a vertical-cavity surface-emitting laser (VCSEL) at 1.68 μm with up to 5 MHz repetition rate," Meas. Sci. Technol. **14,** 101–106 (2003).
5. C. Chang-Hasnain, "Tunable VCSEL," IEEE J. Sel. Top. Quantum Electron. **6**, 978–987 (2000).
6. J. S. Harris, Jr., "Tunable long-wavelength vertical-cavity lasers: the engine of next generation optical networks," IEEE J. Sel. Top. Quantum Electron. **6**, 1145–1160 (2000).
7. M. Lackner, M. Schwarzott, F. Winter, B. Kögel, S. Jatta, H. Halbritter, and P. Meissner, "CO and CO_2 spectroscopy using a 60 nm broadband tunable MEMS-VCSEL at 1.55um," Opt. Lett. **31**, 3170–3172 (2006).
8. B. Kögel, H. Halbritter, S. Jatta, M. Maute, G. Böhm, M.-C. Amann, M. Lackner, M. Schwarzott, F. Winter, and P. Meissner, "Simultaneous spectroscopy of NH_3 and CO using a > 50 nm continuously tunable MEMS-VCSEL," IEEE Sens. J. **7**, 1483–1489 (2007).
9. H. P. Zappe, M. Hess, M. Moser, R. Hövel, K. Gulden, H.-P. Gauggel, and F. Monti di Sopra, "Narrow-linewidth vertical-cavity surface-emitting lasers for oxygen detection," Appl. Opt. **39**, 2475–2479 (2000).
10. P. Vogel and V. Ebert, "Near shot noise detection of oxygen in the A-band with vertical-cavity surface-emitting lasers," Appl. Phys. B **72**, 127–35 (2001).
11. G. D. Cole, E. Behymer, L. L. Goddard, and T. C. Bond, "Fabrication of suspended dielectric mirror structures via xenon difluoride etching of an amorphous germanium sacrificial layer," J. Vac. Sci. Technol., B **26**, 593–597 (2008).
12. G. D. Cole, E. S. Björlin, Q. Chen, C.-Y. Chan, S. Wu, C. S. Wang, N. C. MacDonald, and J. E. Bowers, "MEMS-tunable vertical-cavity SOAs," IEEE J. Quantum Electron. **41**, 390–407 (2005).
13. M. Maute, G. Böhm, M.-C. Amann, B. Kögel, H. Halbritter, and P. Meissner, "Long-wavelength tunable vertical-cavity surface-emitting lasers and the influence of coupled cavities," Opt. Express **13**, 8008–8014 (2005), http://www.opticsinfobase.org/abstract.cfm?URI=oe-13-20-8008.
14. M. Maute, B. Kögel, G. Bohm, P. Meissner, and M.-C. Amann, "MEMS-tunable 1.55-μm VCSEL with extended tuning range incorporating a buried tunnel junction," IEEE Photon. Technol. Lett. **18**, 688–690 (2006).
15. F. Rinaldi, J. M. Ostermann, A. Kroner, and R. Michalzik, "High-performance AlGaAs-based VCSELs emitting in the 760 nm wavelength range," Opt. Commun. **270**, 310–313 (2007).

#98569 - $15.00 USD Received 11 Jul 2008; revised 16 Sep 2008; accepted 16 Sep 2008; published 2 Oct 2008

16. G. D. Cole, J. E. Bowers, K. L. Turner, and N. C. MacDonald, "Dynamic characterization of MEMS-tunable vertical-cavity SOAs," in Proceedings of IEEE/LEOS International Conference on Optical MEMS and Their Applications (MOEMS 2005), Oulu, Finland, 1–4 August 2005, paper F4.
17. A. Syrbu, V. Iakovlev, G. Suruceanu, A. Caliman, A. Rudra, A. Mircea, A. Mereuta, S. Tadeoni, C.-A. Berseth, M. Achtenhagen, J. Boucart, and E. Kapon, "1.55-μm optically pumped wafer-fused tunable VCSELs with 32-nm tuning range," *IEEE Photon. Technol. Lett.* **16**, 1991–1993 (2004).
18. F. Riemenschneider, M. Maute, H. Halbritter, G. Böhm, M.-C. Amann, and P. Meissner, "Continuously tunable long-wavelength MEMS-VCSEL with over 40-nm tuning range," IEEE Photon. Technol. Lett. **16**, 2212–2214 (2004).
19. N. Kanbara, S.-i. Tezuka, and T. Watanabe, "MEMS tunable VCSEL with concave mirror using the selective polishing method," in Proceedings of IEEE/LEOS International Conference on Optical MEMS and Their Applications (MOEMS 2006), Big Sky, MT, 21–24 August 2006, paper MA3.
20. T. Kitano, S. Izumi, H. Minami, T. Ishikawa, K. Sato, T. Sonoda, and M. Otsubo, "Selective wet etching for highly uniform GaAs/$Al_{0.15}Ga_{0.85}$As heterostructure field effect transistors," J. Vac. Sci. Technol. B **15**, 167–170 (1997).
21. G. D. Cole, E. S. Björlin, C. S. Wang, N. C. MacDonald, and J. E. Bowers, "Widely tunable bottom-emitting vertical-cavity SOAs," IEEE Photon. Technol. Lett. **17**, 2526–2528 (2005).
22. P. B. Chu, J. T. Chen, R. Yeh, G. Lin, J. C. P. Huang, B. A. Warneke, and S. J. Pister, "Controlled pulse-etching with xenon difluoride," 9th International Conference on Solid State Sensors and Actuators, Digest of Technical papers Transducers '97, Chicago, IL, USA, paper 2D3.01, pp. 665–668.
23. G. D. Cole and E. Behymer, "Rapid sacrificial germanium etching using xenon difluoride," in Technical Digest of Hilton Head 2008: Solid-State Sensors, Actuators, and Microsystems Workshop, 1–5 June 2008, Hilton Head Island, SC, pp. 388–389.
24. M.C. Larson, A.R. Massengale, and J.S. Harris, "Continuously tunable micromachined vertical cavity surface emitting laser with 18 nm wavelength range," Electron. Lett. **32**, 330–332 (1996).
25. Y. Matsui, D. Vakhshoori, P. Wang, P. Chen, C.-C. Lu, M. Jiang, K. Knopp, S. Burroughs, and P. Tayebati, "Complete polarization mode control of long-wavelength tunable vertical-cavity surface-emitting lasers over 65-nm tuning, up to 14-mW output power," IEEE J. Quantum Electron. **39**, 1037–1048 (2003).
26. K. L. Turner, P. G. Hartwell, and N. C. Macdonald, "Multi-dimensional MEMS motion characterization using laser vibrometry," 10th International Conference on Solid State Sensors and Actuators, Digest of Technical papers Transducers '99, Sendai, Japan, pp. 1144–1147.
27. P. Tayebati, P. D. Wang, D. Vakhshoori, C. C. Lu, M. Azimi, and R. N. Sacks, "Half-symmetric cavity tunable microelectromechanical VCSEL with single spatial mode," IEEE Photon. Technol. Lett. **10**, 1679–1681 (1998).
28. M. C. Y. Huang, Y. Zhou, and C. J. Chang-Hasnain, "A nanoelectromechanical tunable laser," Nature Photonics **2**, 180–184 (2008).

1. Introduction

Vertical-cavity surface-emitting lasers (VCSELs) have attracted considerable interest for a diverse suite of applications, ranging from telecommunications to spectroscopy. In the latter function, the frequency stability, low power consumption, and compact nature of VCSELs lead to a number of advantages over existing semiconductor laser technologies for use in diode-laser-based absorption spectroscopy [1-4]. For spectroscopic use, wavelength tuning in a typical fixed-cavity VCSEL is realized by varying the laser injection current, leading to heating of the structure and a thermally induced red-shift of the emission wavelength, typically less than 3 nm. Progressing beyond fixed-cavity lasers, widely-tunable VCSELs incorporating integrated actuators based on microelectromechanical systems (MEMS) technology have been developed [5]. With MEMS-tunable VCSELs, wavelength tuning is realized through the actuation of a suspended Bragg reflector, resulting in physical variation of the optical path length and wavelength tuning ranges on the order of tens of nanometers. Given the short axial length of a typical VCSEL, displacement of the suspended mirror is capable of producing continuous tuning of a single lasing mode. Originally envisioned as next-generation sources for optical data transmission [6], these devices have recently shown promise as a high-performance alternative to standard VCSELs for optical gas sensing, with demonstrations of the detection of carbon monoxide and carbon dioxide [7], as well as ammonia [8], at the telecom-relevant wavelength range near 1550 nm.

Following this path of research, we have developed the first MEMS-tunable VCSELs with emission wavelengths below 800 nm. These devices operate within the oxygen A-band (760−780 nm), a relevant wavelength range for diode-laser-based oxygen detection [9, 10]. In

#98569 - $15.00 USD Received 11 Jul 2008; revised 16 Sep 2008; accepted 16 Sep 2008; published 2 Oct 2008

these devices, rapid and wide wavelength tuning is realized through the use of an electrostatically actuated micromechanical Bragg reflector. Here, we make use of a novel fabrication method based on gas-phase etching of a room-temperature deposited amorphous-germanium (α-Ge) sacrificial layer to generate the suspended mirror [11]. We present the characterization of our initial demonstration devices with notable results including the potential for a wavelength tuning range of 30 nm, with scan rates up to 1 MHz. Currently, these devices exhibit multimode lasing operation between 767 and 737 nm. With an improved output power and single-mode emission, short wavelength MEMS-tunable VCSELs should be extremely attractive as widely-tunable swept sources for oxygen sensing.

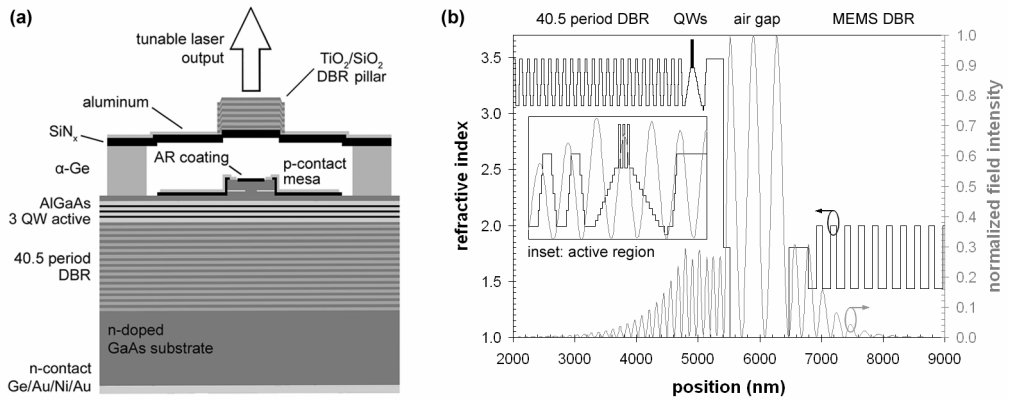

Fig. 1. Design of the short wavelength MEMS-tunable VCSELs. (a) Schematic cross-section of the full materials structure. The non-planarity in the suspended membrane arises from the transfer of the mesa geometry through the evaporated Ge film. (b) Refractive index profile and electric field intensity generated with a transmission matrix model. Note that the composition grading is continuous, but is represented as discrete steps in order to simplify the simulation.

2. Device design

The short-wavelength MEMS-tunable VCSELs presented in this manuscript combine an epitaxial "half VCSEL"—consisting of the bottom distributed Bragg reflector (DBR) and active region—with a suspended micromechanical Bragg reflector that allows for dynamic cavity length variation. In order to reduce the limitations imposed by coupled-cavity effects, these devices utilize an extended cavity (EC) tuning structure as described in Refs. 12 and 13. With the EC-design, the epitaxial half-VCSEL is anti-reflection (AR) coated in order to eliminate the Fresnel reflection from the semiconductor-air interface. Thus, the tunable VCSEL consists of a single distributed cavity combining the epitaxial gain medium and air gap. The use of the EC-design has recently resulted in the demonstration of electrically-injected long-wavelength MEMS-VCSELs with tuning ranges exceeding 60 nm [14]. Carrier and lateral optical confinement in our short-wavelength lasers is realized with an oxide aperture, while an intracavity contact is used below the suspended mirror for current injection into the semiconductor active region. The details of the laser and MEMS materials structure are described in the following subsections; a schematic of the overall design, as well as the refractive index profile and standing wave pattern, is shown in Fig. 1.

2.1 Laser epitaxial structure

The epitaxial structure for the short-wavelength tunable VCSELs is based entirely on the AlGaAs materials system and is deposited via metal organic chemical vapor deposition on 3-inch-diameter n-type GaAs substrates. The design of the AlGaAs half-VCSEL is based in part on the structure developed by Rinaldi et al. [15], with a desired emission wavelength near 760 nm. Due to the strong fundamental absorption of the GaAs substrate in this wavelength range, these devices are constrained to be top-emitting, in this case through the MEMS-tunable

#98569 - $15.00 USD Received 11 Jul 2008; revised 16 Sep 2008; accepted 16 Sep 2008; published 2 Oct 2008

mirror structure. The bottom mirror of our tunable VCSELs consists of a uniformly n-doped (silicon at 2×10^{18} cm^{-3}) 40.5 period DBR with linear composition grading between the high index ($Al_{0.30}Ga_{0.70}As$) and low index ($Al_{0.92}Ga_{0.08}As$) layers. The active region comprises three 8-nm-thick $Al_{0.135}Ga_{0.865}As$ quantum wells (QWs) separated by 10-nm-thick $Al_{0.40}Ga_{0.60}As$ barriers, with a photoluminescence peak designed for 750 nm. Current confinement is provided by a graded high aluminum content oxidation layer, which sits below a p-doped (carbon at 2×10^{18} cm^{-3}) $Al_{0.30}Ga_{0.70}As$ lateral current spreader, with an optical thickness of $3\lambda/2$ (approximate physical thickness of 285 nm). Finally, the cavity is capped with a highly doped (carbon at $>2\times10^{19}$ cm^{-3}) 20-nm-thick p-type GaAs contact layer. The standing wave profile and refractive index as a function of position for this structure is depicted in Fig 1(b); note that composition grading is used to smooth the transitions between the various heterojunctions. Furthermore, as can be seen in the inset of the same figure, the materials structure is carefully designed to ensure that the oxide aperture resides at a null in the electric field, while the QWs are centered on an antinode for maximum enhancement factor.

2.2 Suspended mirror structure

The tunable mirror structure for these devices incorporates only low-temperature deposited dielectric films. From the top down, the suspended mirror consists of an evaporated dielectric TiO_2/SiO_2 DBR (devices are fabricated with 9−13 periods) supported by a composite aluminum and silicon nitride (SiN_x) membrane, with the SiN_x layer acting as a high index quarter-wave film. To achieve adequate mechanical characteristics, the SiN_x film is roughly 320 nm in thickness ($3\lambda/4$ optical thickness at 760 nm). The dielectric mirror structure is suspended above a $5\lambda/4$ air gap which serves as part of the composite cavity. In order to realize the EC-design, a $\lambda/4$ SiN_x AR coating is included at the interface between the semiconductor structure and air gap. Including the AR coating on the surface of the half-VCSEL results in a linear tuning response by eliminating interference effects induced by the intra-cavity reflector [12]. With the large index discontinuity between the air gap and SiN_x membrane, the theoretical peak reflectivity of the top DBR is calculated to be 99.64% and 99.97% for 9 and 13 periods, respectively. For comparison, the estimated reflectance of the bottom DBR considering absorption due to free carrier loss is 99.86%. It is important to note that the estimates for the dielectric DBR assume no scattering or absorption loss; realistically, the low quality of the evaporated films will reduce the achievable reflectivity.

To enable continuous tuning of the laser emission wavelength, the suspended mirror incorporates an integrated electrostatic actuator. In this implementation an applied bias across the aluminum contact on top of the SiN_x structural film and the p-contact pad on the VCSEL creates an electrostatic force that displaces the suspended mirror towards the substrate, reducing the optical path length and blue-shifting the resonance wavelength. The use of electrostatic actuation allows for a rapid tuning response. Previous characterization of devices utilizing the same micromechanical layout has demonstrated a near critically-damped response at atmospheric pressure with a settling time below 10 μs [16].

3. Device fabrication

The fabrication procedure for the short-wavelength MEMS-tunable VCSELs is a relatively complex process involving up to 12 lithographic levels for wire-bond enabled devices. Although wafer scale processing is possible, for the work presented here, the devices are processed in arrays (device center-to-center spacing of 630 μm) on 1 in. by 1 in. chips in order to conserve valuable epi-material. As with fixed-cavity VCSELs, these devices allow for on-wafer testing throughout the process. For organizational purposes, we describe the details of the microfabrication procedure in two subsections. It is important to note that these devices are fully-monolithic; in this design the MEMS-tunable mirror is integrated as a thin film structure on the surface of the half-VCSEL, and does not require wafer bonding [17] or the assembly of disparate chips [18, 19]. A schematic of the process flow is included in Fig. 2.

#98569 - $15.00 USD Received 11 Jul 2008; revised 16 Sep 2008; accepted 16 Sep 2008; published 2 Oct 2008

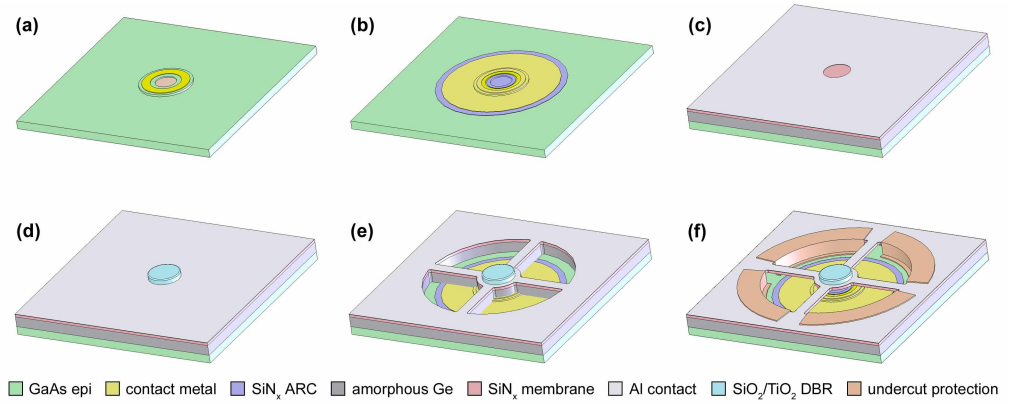

Fig. 2. Schematic of the short-wavelength MEMS-tunable VCSEL process flow. (a) Mesa etch, AlGaAs oxidation, p-contact metallization, and contact window etch. (b) Definition of the SiN_x AR coating and Ti/Au pad. (c) Deposition of the α-Ge sacrificial layer, SiN_x membrane, and aluminum top contact, followed by patterning of the emission window. (d) Blanket SiO_2/TiO_2 DBR evaporation and etch back. (e) ECR etch of actuator geometry. (f) Liftoff of SiO_2 undercut protection and release by sacrificial germanium etching in XeF_2.

3.1 Half-VCSEL

Processing begins with the definition of the oxide aperture that provides both current and lateral optical confinement for the laser. In order to expose the high-Al-content oxidation layer, a non-selective wet chemical etching process consisting of H_3PO_4:H_2O_2:H_2O at a ratio of 1:5:15 is used to define a shallow mesa through the GaAs contact layer and $Al_{0.30}Ga_{0.70}As$ current spreader. After thoroughly cleaning the sample, oxidation is carried out at 430º C in a N_2/H_2O ambient. The etched mesa is 50 µm in diameter, requiring lateral oxidation distances of approximately 20 µm (oxide apertures range from 5 to 7 µm in diameter for the devices presented here). Following oxidation, a Ti/Pt/Au annulus is deposited via electron-beam evaporation on the highly-doped GaAs p-contact layer. Next, a blanket Ge/Au/Ni/Au n-contact stack is evaporated on the sample backside. Rapid thermal annealing at 350º C is performed to generate ohmic contacts to the semiconductor structure.

To reduce optical loss in the cavity, a window is defined in the absorbing GaAs contact layer using a highly-selective wet etch based on a buffered citric acid solution ($C_6H_8O_7/NH_4OH/H_2O_2$). This process allows for the removal of the binary GaAs over the ternary current spreader with excellent selectivity [20]. The exposed $Al_{0.30}Ga_{0.70}As$ layer is then capped with a quarter-wave SiN_x film deposited by plasma enhanced chemical vapor deposition (PECVD) and patterned with a CF_4/O_2 plasma etch. This film serves numerous purposes: 1) it acts as an AR coating to create the extended cavity tuning structure, 2) it inhibits oxidation of the exposed $Al_{0.30}Ga_{0.70}As$, and 3) it serves as an isolation layer for the p-contact pad to be added in the following process step. To complete the half-VCSEL structure, an evaporated Ti/Au contact pad is patterned by liftoff. This pad contains an optical aperture in the center and overlaps with the original Ti/Pt/Au contact metal, enabling current injection into the p-doped oxide-confined mesa. Furthermore, this film acts as the ground electrode for the MEMS actuator. Subsequent to the completion of the half-VCSEL, preliminary characterization of the laser structure may be performed including electroluminescence (EL) and current-voltage measurements.

3.2 Suspended Bragg reflector

The suspended mirror for our MEMS-VCSELs utilizes a nearly identical mechanical design (i.e. mask layout) to wavelength tunable vertical-cavity semiconductor optical amplifiers demonstrated previously [21]. As opposed to the all-epitaxial MEMS-VCSOAs, the devices presented here utilize a dielectric structure for the actuator. Fabrication of the suspended mirror begins with the evaporation of a 1-µm-thick α-Ge sacrificial layer on top of the

#98569 - $15.00 USD Received 11 Jul 2008; revised 16 Sep 2008; accepted 16 Sep 2008; published 2 Oct 2008

completed half-VCSEL. The details of this deposition process, in addition to an in-depth description of the tunable mirror fabrication steps, are presented in [11]. For completeness, this process will be reviewed here. Following the α-Ge evaporation, a SiN_x structural film is deposited in a second PECVD process. Because this film serves as the first high index layer in the suspended DBR, the optical thickness is constrained to be an odd-multiple of a quarter-wave. In this case we use $3\lambda/4$ (physical thickness of approximately 320 nm), which, when coupled with the slight tensile stress in the film, provides sufficient mechanical properties for the membrane. Next, a 1500-Å-thick aluminum top contact layer is evaporated over the SiN_x. After evaporation, a window is opened in the aluminum by wet chemical etching, allowing for optical transmission through the opaque contact layer, as with the lower Ti/Au electrode. A blanket electron-beam evaporation of alternating quarter-wave SiO_2/TiO_2 forms the remainder of the dielectric reflector and completes the materials structure for the suspended mirror.

Following the mirror deposition process, the DBR pillar is defined by electron cyclotron resonance (ECR) etching of the TiO_2/SiO_2 stack with a SF_6/Ar chemistry, with the aluminum top contact serving as an excellent etch stop. Next, the actuator geometry is defined by wet chemical etching through the aluminum film, and then dry etching through the SiN_x membrane and α-Ge sacrificial layer with a CF_4/O_2 ECR etch. In this case the gold contact pad and GaAs substrate serve as an etch stop. Next, a low-temperature (100º C) SiO_2 film is deposited in a third PECVD process and patterned via liftoff. This feature serves to eliminate etching of the sacrificial layer beneath the outer-lying support structure and improves the control over the unbiased air-gap thickness [12]. An image of a device taken just prior to release can be seen in Fig. 3.

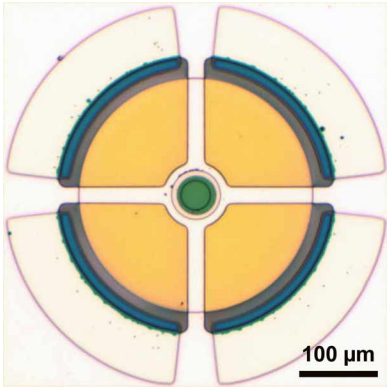

Fig. 3. Optical micrograph of an individual tunable VCSEL prior to the XeF_2 undercut process.

To complete the fabrication sequence, the sacrificial α-Ge layer is selectively etched by exposing the sample to 1 Torr of XeF_2 in a pulsed etching system [22]. This process enables rapid dry etching of the α-Ge sacrificial layer and exhibits a number of advantages when compared with other candidate micromachining techniques. On one hand, it allows for real-time observation of the release etch due to the simplicity of the non-plasma etch system. As a second benefit, the gas-phase etching process alleviates the need for critical point drying, in contrast to wet-chemistry-based undercut etching where surface tension forces may collapse the suspended mirror structure. The most interesting aspect of this fabrication method is the particularly rapid nature of the under-etching process: for a XeF_2 etch pressure of 1 Torr, the evaporated α-Ge film exhibits lateral etch rates exceeding 150 µm/min [23]. For the devices presented in this manuscript, the total time required to successfully undercut an 80-µm diameter membrane was less than 20 seconds.

#98569 - $15.00 USD Received 11 Jul 2008; revised 16 Sep 2008; accepted 16 Sep 2008; published 2 Oct 2008

4. Results and discussion

Measurements of the EL spectrum of the AR coated half-VCSELs were performed at room temperature using a cleaved multimode fiber (50 μm diameter core) for light collection, sent to an optical spectrum analyzer (OSA) for analysis. As shown in the example in Fig. 4, the EL peak is centered at 756.4 nm, with a full width at half maximum of 20.4 nm for a continuous wave (CW) drive current of 3 mA. Micro-reflectance characterization of a completed tunable VCSEL performed with a microscope-coupled visible spectrometer (400-800 nm) show cavity resonances at roughly 778 nm and 741 nm (note that the bandwidth of the epitaxial DBR is 54 nm). Measurements from a number of devices show an average free spectral range (FSR) of 36 nm. This value is similar to the theoretical FSR results generated with a transmission matrix model, as in Fig. 1(b). This simulation predicts resonances at 778.5 nm and 738.5 nm for an air-gap thickness of 1100 nm. For the suspended mirror we estimate the reflectance to be 99.5% for the 9.5 period suspended mirror structure and exceeding 99.8% at 13.5 periods. We also observe a lack of repeatability in the DBR evaporation process. For example, in the 13 period deposition the center wavelength of the mirror was nearly 50 nm short of the desired center wavelength. Fortunately, the stopband of the dielectric mirror exceeds 150 nm, making the overall cavity resonance quite tolerant to a lack of thickness control in the suspended mirror structure.

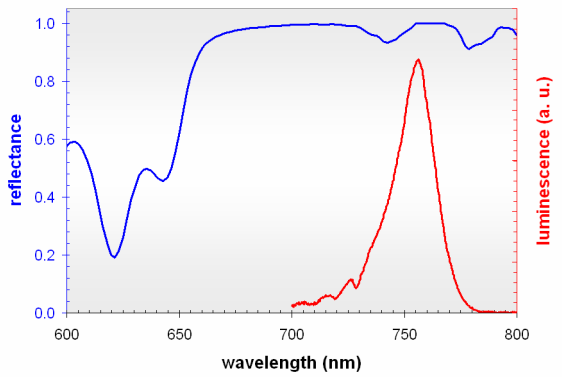

Fig. 4. Microreflectance (blue line) overlaid with the EL spectrum (red) for a completed MEMS-tunable VCSEL. The FSR in this case is 37 nm, with the long wavelength resonance red-shifted 22 nm with respect to the luminescence peak.

Next, we characterize the current-voltage and light output characteristics of our tunable VCSELs. As seen in Fig. 5, the half-VCSEL structure shows a substantial differential resistance of nearly 2.8 kΩ, leading to excessive voltages of up to 10 V at 3 mA. Transmission line measurements made on the same epitaxial materials structure produce an average contact resistance of roughly 7×10^{-6} Ω·cm^2. Using a conservative estimate of the contact resistance of 1×10^{-5} Ω·cm^2, the 1068 μm^2 p-contact area yields a resistance of less than 1 Ω from the ring contact. We postulate that the excess resistance is due in large part to the thin current spreading layer. Unfortunately, this high resistance leads to significant internal heating and limits the devices to drive currents below 5 mA.

Also shown in the figure is the typical light output power versus injection current for a 13.5 period sample (aperture diameter of 5 μm). Threshold in this device is estimated to be 400 μA. Included in the inset is the spectrum for a current of 2.5 mA and MEMS bias of 10 V. These devices exhibit very low output powers, with broad area photodetector measurements yielding a typical peak power around 10 μW. This performance is similar to early 980-nm tunable VCSELs developed by Larson et al. [24], but falls far short of the high output power 760-nm fixed-cavity VCSELs demonstrated by Rinaldi et al. [15]. In addition to the excessive resistance and resulting Joule heating, the low output power is also attributed to the high reflectivity of the suspended mirror structure; in this case, a significant portion of the power

#98569 - $15.00 USD Received 11 Jul 2008; revised 16 Sep 2008; accepted 16 Sep 2008; published 2 Oct 2008

may be lost to the highly absorbing substrate. Additionally, we find that these lasers show extremely short lifetimes under room-temperature CW operation, typically a few minutes, and in the best cases approximately 1 hour. Aside from the internal heating, we are also concerned about the placement of the oxidation layer in this materials structure. With our current design, the center of the AlO_x layer is only 130 nm away from the QWs; the high strain generated at the interface with the oxidized layer may be a contributing factor to the degradation of the devices.

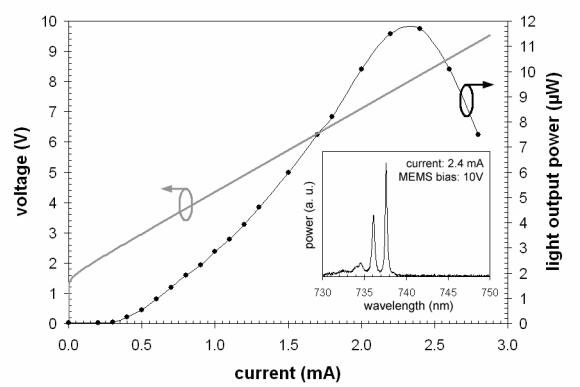

Fig. 5. Voltage and light output as a function of drive current for a MEMS-tunable VCSEL with a 13.5 period suspended mirror structure. The inset includes the spectral characteristics near roll-over. Note that this device is multimode over the current range shown.

The wavelength tuning results for a large aperture (7-μm diameter) multimode MEMS-VCSEL are included in Fig. 6. Lasing operation was not achieved in this device until the bias on the electrostatic actuator reached 12 V. For a CW drive current of 2 mA, a 6.2 nm tuning range was recorded, from 761.9 to 755.7 nm, corresponding to actuation voltages between 10 and 20 V. At 12 V the threshold current for this laser was found to be approximately 750 μA. Tuning was ultimately limited by excess leakage current in the MEMS structure; although regardless of the displacement limitation, beyond 755 nm it appeared that lasing threshold could no longer be reached. Regarding the limitations to the tuning range, we have found that devices capable of reaching the full extent of displacement, i.e. to the point of physical contact with the mesa, exhibit a minimum wavelength near 736 nm. With the hope of extending the tuning range (in this case assuming that the reflectance of the 9.5 period DBR was insufficient), additional devices were fabricated with 13.5 period suspended mirror structures.

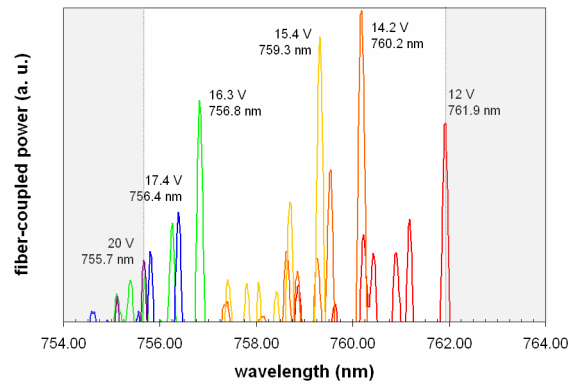

Fig. 6. Tuning response for a 7-μm aperture MEMS-tunable VCSEL for a constant laser drive current of 2 mA. Lasing operation occurs within the non-shaded region in the plot, covering over 6 nm from 761.9–755.7 nm.

#98569 - $15.00 USD Received 11 Jul 2008; revised 16 Sep 2008; accepted 16 Sep 2008; published 2 Oct 2008

An example of a tunable VCSEL capable of the full range of motion is shown in Fig. 7. This structure has a reduced aperture diameter of 5 μm and although remaining multimode, it displays slightly improved spectral characteristics, as in the inset of Fig. 5. In this device the unbiased cavity resonance occurs at 767.0 nm (simulated air-gap thickness of 1004 nm). Under these conditions there is no second mode within the high reflectivity band of the epitaxial DBR, allowing for mode-hop-free resonance tuning from 767.0 nm to 736.5 nm. Furthermore, the position of this mode results in almost ideal alignment with the gain peak. Unfortunately, the laser exhibits a significant variation in output power and it is not clear that lasing operation is maintained over the entirety of the 30-nm span—particularly between 755 and 745 nm. Additionally, the large wavelength jump from 744.4 to 737.6 nm (relating to applied MEMS biases between 10 and 10.5 V) is indicative of the snapdown instability of the electrostatic actuator. As a positive note, it turns out that stiction of the suspended structure is alleviated in these devices, as the SiN_x does not permanently adhere to the gold surface on top of the mesa and repeatedly springs back after a reduction in the voltage. Even with the obvious limitations, these results demonstrate that, with minor improvements, it should be possible to achieve continuous lasing operation over the full FSR for EC-design short-wavelength tunable VCSELs. Note that the 30 nm range in these devices corresponds to 4% of the laser operating wavelength, which is equivalent to tuning ranges approaching 70 nm (4.5% for emission at 1550-nm) for long-wavelength MEMS-tunable VCSELs [14, 25].

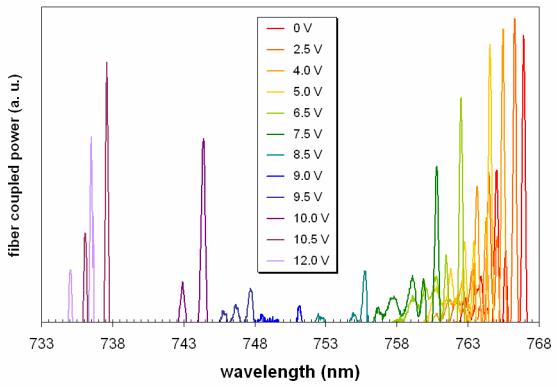

Fig. 7. Tuning response for a 13.5 period MEMS-tunable VCSEL for a constant laser drive current of 2.4 mA. Lasing operation occurs discontinuously over a range of 30 nm, from 767–737 nm. It is assumed that the cessation of lasing operation is due to additional loss within the cavity arising from non-uniform deflection of the suspended mirror.

To investigate the electromechanical response of the actuator, we employ a MEMS motion characterization system consisting of a microscope-coupled laser Doppler vibrometer (LDV) [26]. The LDV enables analysis of the velocity and displacement of the suspended mirror under various driving conditions, facilitating measurements such as the displacement as a function of bias, as well as the mechanical frequency response. An example of the step response and static displacement characteristics of the suspended mirror can be found in Ref. 11. Combining static displacement measurement (deflection versus voltage) with the emission wavelength as a function of applied bias (as shown in Fig. 8), it is possible to ascertain the resonant wavelength shift of the optical cavity as a function of the physical displacement of the suspended mirror. For the widely tunable device, the conversion from physical displacement to resonance tuning is 0.12. In these devices the addition of the intra-cavity AR coating results in a linear tuning response with respect to the change in air-gap thickness (see inset of Fig. 8), as expected with the EC-design [12, 13].

#98569 - $15.00 USD Received 11 Jul 2008; revised 16 Sep 2008; accepted 16 Sep 2008; published 2 Oct 2008

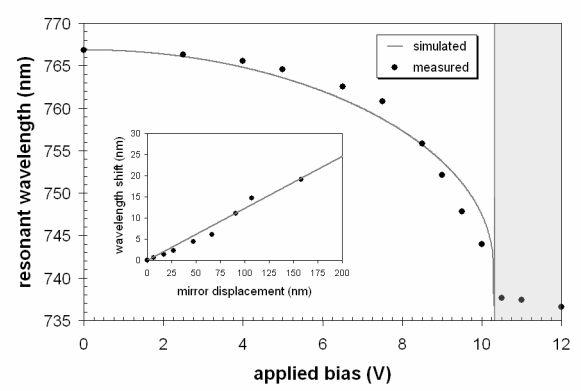

Fig. 8. Theoretical (solid line) and experimental (points) optical resonance as a function of the applied bias. The shaded region beyond 10 V indicates the unstable regime for the actuator. Combining this dataset with LDV-based measurements of the suspended mirror, it is possible to extract the wavelength shift as a function of the physical displacement of the suspended mirror. In this device the theoretical tuning response (included as the solid line in the inset) is approximately 12 nm of wavelength shift for 100 nm of displacement of the suspended mirror.

Focusing on the dynamic properties of the suspended mirror, we record a near ideal critically-damped mechanical frequency response under sinusoidal excitation at atmospheric pressure, with typical mechanical resonance frequencies between 0.5 and 1.0 MHz. The details for this testing procedure can be found in Ref. 16. The results shown in Fig. 9 are for a suspended mirror with 80-µm long by 20-µm wide springs, with a central plate diameter of 80-µm. This device exhibits a damped resonance near 700 kHz, with a mechanical quality factor (Q) of 0.74 (ideal critical damping will yield a Q of 0.5). Note that this suspended mirror has a mechanical bandwidth in excess of 1 MHz. These results verify that electrostatically-actuated MEMS-tunable VCSELs are promising candidates for high-speed swept sources in spectroscopic applications.

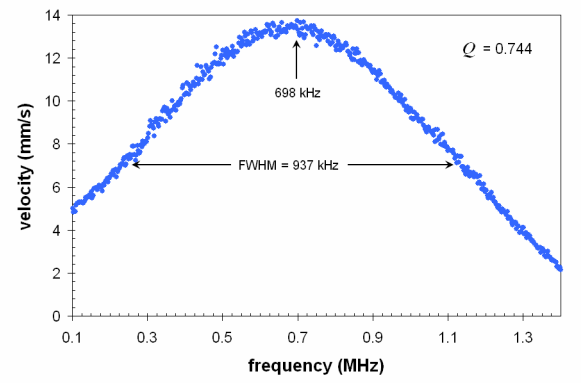

Fig. 9. Typical frequency response for a 13.5 period suspended mirror structure at atmospheric pressure (geometry described in text). Due to the large ratio of lateral dimensions to air-gap thickness, damping is dominated by squeeze film effects. The actuator examined here exhibits a mechanical resonance at 698 kHz with a Q of 0.74. For continuous scanning applications this device can sweep the desired tuning range at rates exceeding 1 MHz, while for step and hold applications, the settling time (defined as ±5% of final displacement) is 850 ns.

6. Conclusions and future outlook

We have outlined the development and demonstration of the first MEMS-tunable VCSELs with emission wavelengths shorter than 800 nm. These devices show the potential for wide

#98569 - $15.00 USD Received 11 Jul 2008; revised 16 Sep 2008; accepted 16 Sep 2008; published 2 Oct 2008

wavelength tuning within the oxygen A-band, making them interesting as high-speed tunable sources for unambiguous O_2 detection. With minor improvements in the epitaxial materials structure, as well as the uniformity of the suspended mirror structure, it should be possible to demonstrate high-performance MEMS-tunable VCSELs with tuning ranges in excess of 4% of the emission wavelength near 760 nm. The contributing factors to the poor performance and short lifetimes of our current short-wavelength MEMS-tunable VCSELs are the excessive resistance arising from the thin current spreading layer, as well as the close proximity between the oxidation layer and QWs.

Furthermore, the output power and spectral characteristics of these lasers must be improved. Although our current devices are multimode, single-mode tunable emission is required for use in spectroscopic applications. For the present design, reduced aperture diameters resulted in poor reliability, from a combination of high series resistance as well from degradation of the active region following oxidation; thus, it was not possible to demonstrate single-mode lasers in this effort. Beyond the obvious improvements, for future work, it would be interesting to investigate structures with advanced suspended mirror geometries. By incorporating a curved mirror structure [27], further improvements in the performance of these devices can be realized. Finally, this fabrication process is amenable to the integration of high index contrast sub-wavelength gratings. These structures have recently been integrated into GaAs-based MEMS-VCSELs, with demonstrations of tuning ranges approaching 20 nm [28]. These normal incidence gratings simplify the suspended mirror structure by reducing the top DBR to a single layer, paving the way for nanosecond tuning in these devices.

Acknowledgments

This work was performed under the auspices of the U.S. Department of Energy by Lawrence Livermore National Laboratory under Contract DE-AC52-07NA27344. GDC acknowledges financial support from the Engineering Relations with Academia (ERA) program at LLNL and thanks Jonathan Geske and Michael MacDougal of Aerius Photonics, LLC, as well as Benjamin Kögel of the Technische Universität Darmstadt for numerous enlightening discussions.

#98569 - $15.00 USD Received 11 Jul 2008; revised 16 Sep 2008; accepted 16 Sep 2008; published 2 Oct 2008